Sub Topic: Internal Combustion and Gas Turbine Engines

10th U. S. National Combustion Meeting
Organized by the Eastern States Section of the Combustion Institute
April 23-26, 2017
College Park, Maryland

Flow Structure Comparison for two 7-Point LDI Configurations

Yolanda R. Hicks[1] and Kathleen M. Tacina[1]*

NASA Glenn Research Center, Cleveland Ohio, USA
[*]Corresponding Author Email: yolanda.r.hicks@nasa.gov

Abstract: This paper presents a comparison primarily of the cold flow 2-D velocity profiles; and describes flame tube combusting flow operability for a 7-point Lean Direct Injector (LDI). This circular LDI array consists of a center element surrounded by six outer elements spaced 60 degrees apart; the spacing between all adjacent elements is the same. Each element consists of a simplex atomizer that injects at the throat of a converging-diverging venturi, and an axial swirler upstream of the venturi throat to generate swirl. The two configurations were: 1) one which consists of all 60° co-swirling axial air swirlers, and; 2) one configuration which uses a 60° swirler in the center, surrounded by counter-swirling 45° swirlers. Testing was done at 5- bar and at an inlet temperature of 700K. Two air reference velocities were considered in the cold flow measurements. The 2D velocity profiles were determined using particle image velocimetry. Results indicate the configuration using all 60°swirlers generates a field that moderates to a more uniform distribution at a shorter distance downstream and is more easily operable than the second configuration, which produces recirculation regions at the edges of the outer 45° swirlers, and results in a more stratified velocity field at any given axial location.
Keywords: fuel-air mixing, lean direct injection, combustor aerodynamics, PIV

1. Introduction

This paper presents recent highlights of results from on-going work to study fluid mixing by varying air swirler angle and center element offset in a 7-element lean direct injector array using cold flow velocity measurements, along with flame structure and operability during combustion,. Reference [1] highlights the first part of a parametric study in which we varied swirler angle and spacing of the 7 element array. One objective of that work was to better understand performance differences between our 9-element and the 7-element array. In the 9-element array, we saw that a central recirculation zone (CRZ) forms downstream of the center swirler element when all swirlers are 60°. In previous work with the 7-element array, the CRZ did not form. In that survey, we determined the element spacing in the 7-point array was too close, so that element interaction likely prevented the formation of a central CRZ; however a CRZ seemed to form downstream of the outer 60° elements. We also did limited testing that showed that if 45° swirlers are in the outer positions, then a CRZ is created downstream of the center 60° element. Reference [2] provides some insight into differences in fields generated using different axial swirler angles.

In this work, we describe the flow from two swirler configurations, namely configuration A, which consisted of all left-hand, 60° swirlers; and configuration B, consisting of a central right-hand, 60° swirler, surrounded by six, right-hand 45° swirlers. We also briefly discuss combustion operability of the two configurations.

2. Methods / Experimental

2.1 LDI hardware

The top of figure 1 shows the components of the LDI element used in these experiments. The air passes through a swirler just before entering a converging-diverging venturi. The air swirlers have an outer diameter of approximately 22-mm, and consist of six helical blades, either right- or left-handed, to generate clockwise or counter-clockwise swirl. The air swirlers used in this study had vane angles of 60° or 45°. At the venturi throat, fuel is injected using a simplex nozzle. This pressure-swirl atomizer was designed to produce a hollow cone spray with a spray angle near 70°. It has a flow number, FN_{US} of about 0.7. A schematic drawing of the 7-point LDI array is shown at the bottom of figure 1. It consists of a center LDI element, surrounded by six elements of equal size. The spacing between adjacent elements is the same, 23.8-mm.

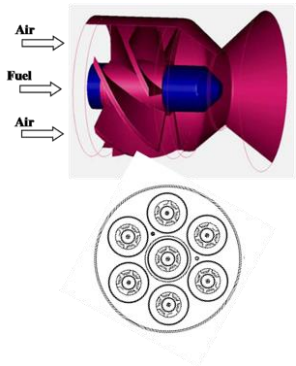

Figure 1: Detail view of a single LDI element; Sketch showing element arrangement of 7-point array.

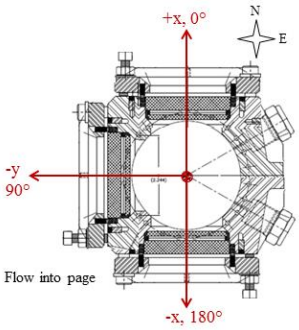

Figure 2: Cross-sectional detail of combustor that shows window orientation, and defines the coordinate system.

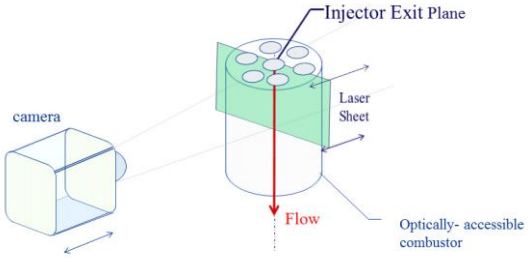

Figure 3: Sketch showing the imaging setup relative to the combustor for PIV measurements.

2.2 Test Facility

The experiments were conducted in the Combustion and Dynamics Facility (CDF), in which the flow passes from top to bottom. The combustor test section is 15-cm long with cross-section 7.62-cm in diameter. Three sets of double-paned windows, spaced 90° apart around its circumference, provide optical access to the water-cooled combustor. The windows are flat and have a small offset away from the combustor circumference. The windows measure 6.1-cm tall (axial direction) by 5.8-cm wide (azimuthal). Figure 2 shows a plan view of the combustor section, and the coordinate system definition.

2.3 Optical Instrumentation and Procedure

We used an imaging layout similar to that illustrated in Figure 3. A laser beam was formed into a light sheet using a set of cylindrical lenses. The sheet passed through the test section and was aligned parallel with the flow direction. The camera was positioned normal to the laser sheet and collected the light scattered by droplets. The PIV data were acquired using a 15-Hz dual-head, frequency-doubled, Nd:YAG laser and a single, interline transfer, CCD camera.

Seeding was achieved using water spray from the center nozzle. This enabled us to heat the air to inlet temperatures we would normally use for combustion tests and match either the volume flow or mass flow rate of the fuel. The advantage of this approach is that the windows stayed clean for the hour or more required to collect the data. Thus, water seeding is far superior to powder or oil seeding. The biggest disadvantage of this approach is that the "seed" is not necessarily uniformly distributed and that in the near field, the water tracks the flow from the nozzle(s) rather than of the air. However, we determined when comparing data from the two seeding approaches that using water gave us the information we were looking for in terms of the bulk fluid motion.

We traversed across the flow, typically in 1-mm increments, collecting 500 image pairs per position. Data were collected at 5-bar, 700K, and two cold flow reference velocities, u_{ref}: 22.9-m/s and 15.2-m/s.

3. Results and Discussion

Brief descriptions of the measured velocity fields follow. Aside from the overall ranges in velocity magnitude for the two reference velocities, the fields were similar for a given swirler configuration. For that reason, we will focus on the case using a reference velocity of 22.9-m/s.

In the combusting tests, we were able to operate stably at the same equivalence ratio, configuration A up to a reference velocity of 16.7-m/s, and configuration B to 13.7-m/s.

3.1 Configuration A—All left-hand 60° swirlers.

Figure 4 shows the mean horizontal-vertical (axial) vector components at three y-positions. Vertical lines indicate array element centerline locations, with a heavy dash-dot if the laser sheet is in the plane, and a faint dashed line otherwise. In addition to the 2D-vector field, the top row shows the axial velocity contour, while the bottom row depicts the axial velocity component using black squares and the RMS of the axial velocity using red squares.

The vector fields show that there is no CRZ formed downstream of the central element near y = 0, but that CRZs are formed downstream of the outer elements within the field of view at y = ± 12. Generally speaking, the RMS of the axial velocity component is proportionally higher near the dome exit (z = 0). Then, within the central core—roughly x ± 12-mm, the RMS decreases relative to the mean velocity, as one moves downstream, indicating the field has become more uniform. The area outside the central core can be subdivided into two regions—with or without recirculation. In the area without recirculation, the RMS and axial velocity components are on the same order. In the recirculation zone, the RMS is often higher than the axial velocity.

To get an overall sense of the velocity field, we constructed a 3D data block merging the velocity data from all the y-positions. This allowed generation of axial velocity contours a various z-positions, shown in figure 5, from the dome exit at z = 0 to z = 35-mm. Black circles the locations of the injector elements at the exit plane. We can observe recirculation behind the elements along y = ± 12 and high downstream velocity from the center element. The z = 0 slice also shows that the high velocity core from the central element is compressed in x so that it is more rectangular than circular. Proceeding downstream, both the recirculation regions and the high central core velocity regions grow in area, and by z = 5 mm, we can see that the high velocity core is bounded by flow from the outer six elements, such that the core is six-sided. At z = 10, we can also see that a recirculation zone is indicated downstream of the remaining two outer elements, at the top and

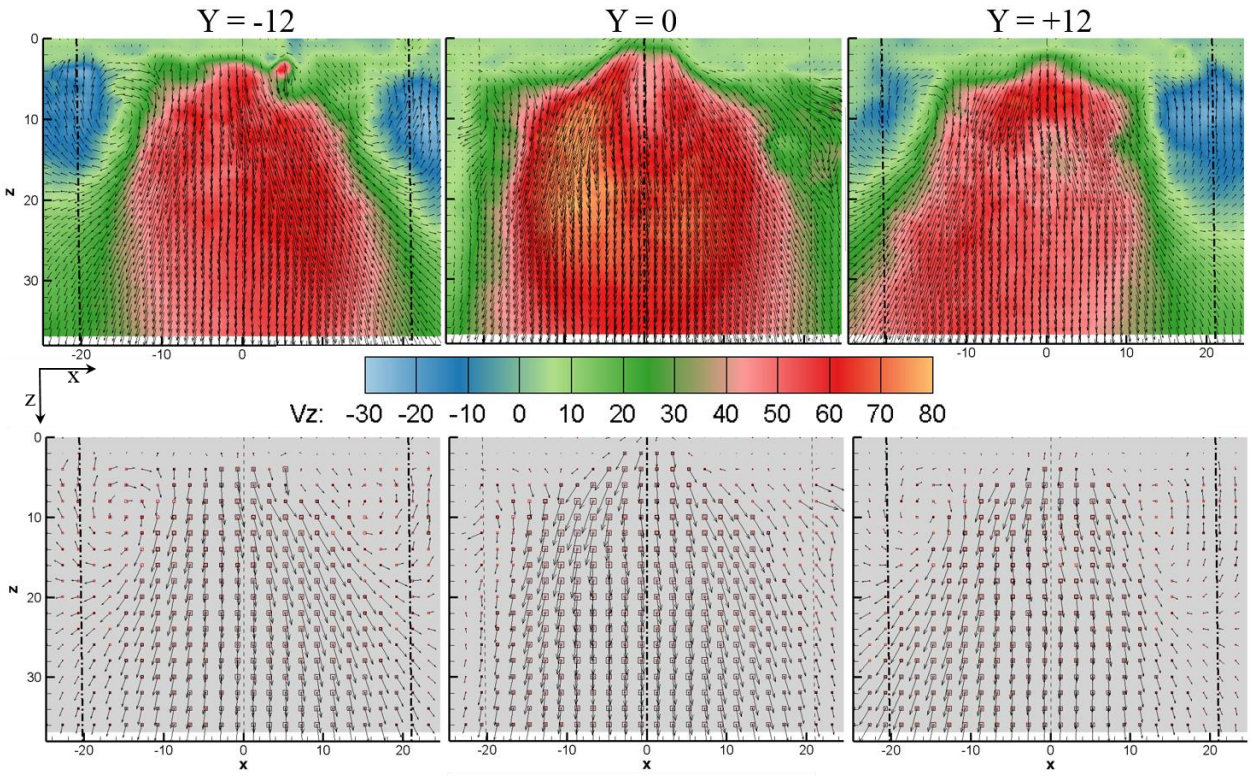

Figure 4: 2D vector field in three y-planes, -12, 0, +12. Top: Vectors with axial velocity contours. Bottom: Vectors and axial component (black squares) and RMS (red squares). Flow from top to bottom.

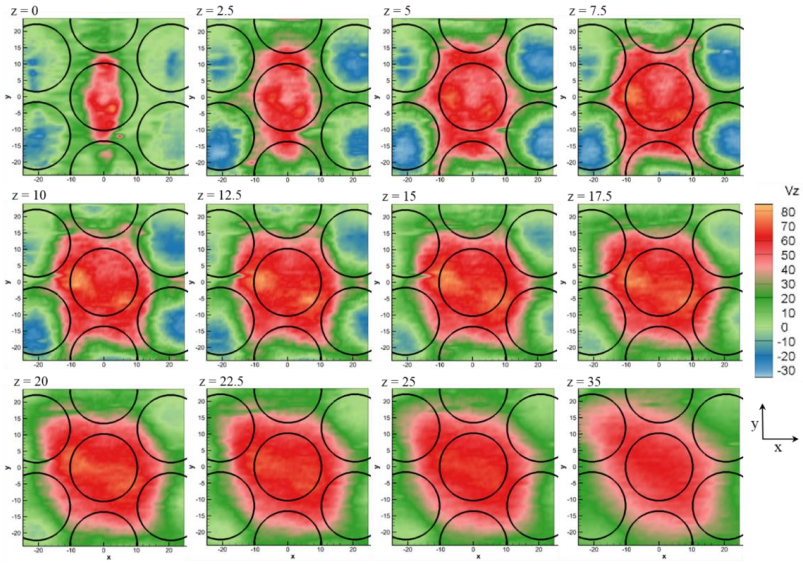

Figure 5: Configuration A result. Contours that show axial velocity within axial slices. The z-location is noted for each slice. U_{ref} = 22.9-m/s.

bottom of the composite image, and near the edge of our field of view (y = ± 24). The CRZs in these two areas are shifted away from their respective centerlines. This corresponds with the compression of the high-velocity core at the center of the array. The maximum reverse flow axial velocity is indicated in the vicinity of z = 5 or 7.5-mm, but a CRZ persists as far as 20-mm downstream. By 22.5-mm, however, all flow proceeds downstream. Another item to note is the overall counterclockwise motion generated by the left-hand air swirlers, which can be seen by focusing on the high velocity core, in red, as one moves downstream from slice to slice.

3.2 Configuration B—Central right-hand 60° swirler with six, outer right-hand 45° swirlers

Figures 6 – 8 show velocity field results from configuration B. In figure 6, we show the average 2D velocity field at y = 0 for both test points. In this configuration, the surrounding 45° swirlers do not expand the flow radially outwards as much as the 60° swirlers do. The flow from the center element is more isolated, and as can be seen in figure 6, a CRZ is produced behind that element. As expected, the higher reference velocity case produces a "stronger" CRZ, but the lower velocity case shows an indication of reverse flow away from the CRZ. Looking at the axial composite slices for test point 2 (figure 8), two key details were revealed near the outer swirlers, whose locations are outlined with red circles. First, the velocity patterns show high downstream velocity for half the area, but much slower positive-going—or even reverse flow for the other half of the area. So, small recirculation zones appear in particular behind the swirlers at the top left and bottom right of the images, and there are indications reverse flow may also be occurring downstream from all of the outer swirlers at some point. This is emphasized in figure 7, in which any region that has reverse flow is shown in white. Second, this stratification of velocity downstream of each outer swirler persists quite far downstream, to 40-mm, depending on the reference velocity. We saw with configuration A that the velocity field distribution had moderated by about 25-mm, by which point the CRZs were gone. We also could not discern a core rotation from configuration B.

4. Summary

Two swirler configurations for a 7-point lean direct injector were compared using 2DPIV: 'A', consisting of all 60° co-swirling axial air swirlers, and; 'B', consisting of a 60° swirler in the center, surrounded by counter-swirling 45° swirlers. For A, axial velocity field behind each swirler tends to be radially symmetric, and the recirculation zones end by 20-mm. For B, the flow behind only the center 60° swirler is symmetric. The outer 45° swirlers present radial asymmetry behind each, including recirculation zones in some cases; and those recirculation zones persist beyond the center element CRZ. Operationally, configuration A can burn stably at a higher reference velocity than can configuration B.

5. Acknowledgements

This work was supported by the Transformational Tools and Technologies Project under the NASA Aeronautics Research Mission Directorate.

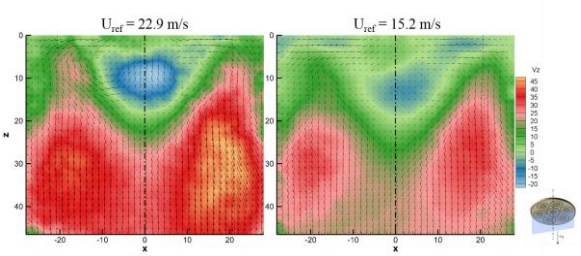

Figure 6: Configuration B result. 2D vector field at y = 0, for the two reference velocities.

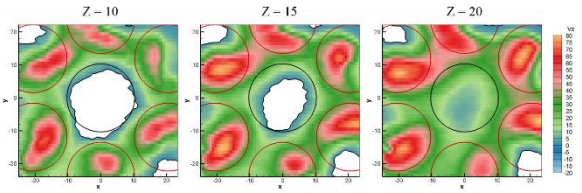

Figure 7: Configuration B result. Axial velocity contour at three axial positions. White highlights the areas with reverse flow. U_{ref} = 22.9-m/s.

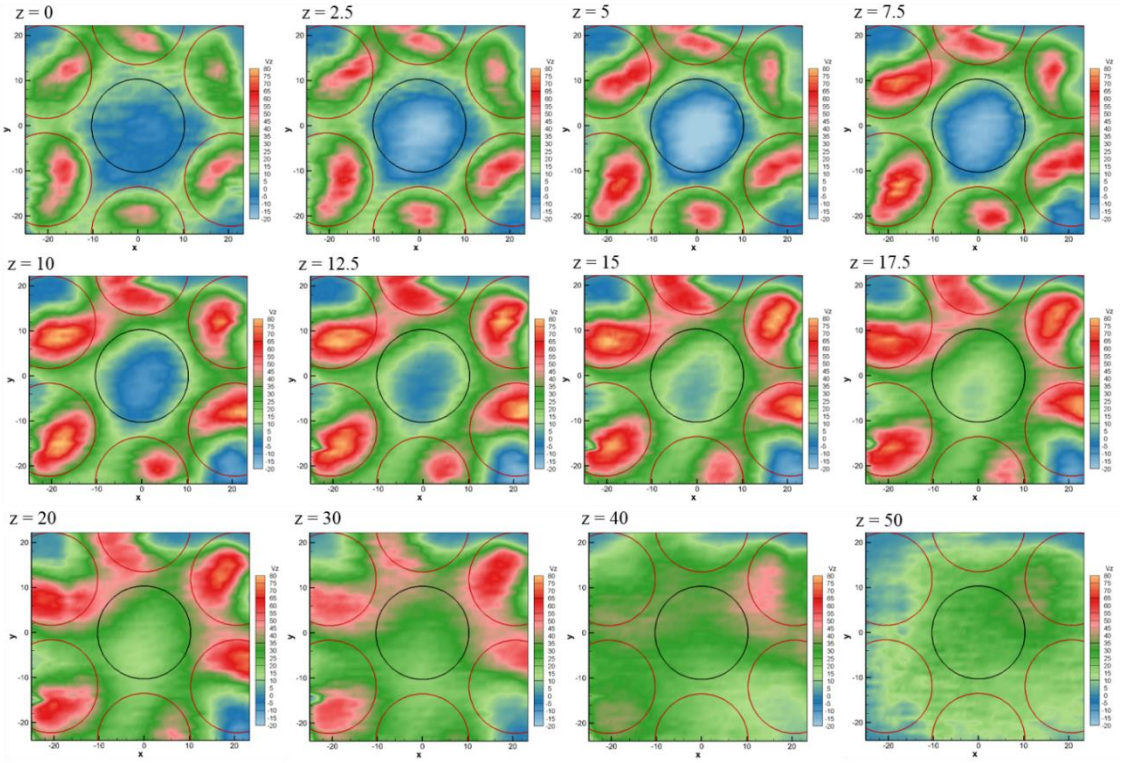

Figure 8: Configuration B result. Contours that show axial velocity within axial slices. The location is noted for each slice. U_{ref} = 22.9-m/s.

6. References

[1] Y.R. Hicks, K.M. Tacina, R.C. Anderson, S.A. Tedder, A comparison of flow fields generated by varying swirler configurations in a 7-point lean direct injector array, 2016 Spring Technical Meeting, Central States Section of the Combustion Institute, Paper 145IC-0035.

[2] K. Ajmani, H.C. Mongia, P. Lee, Evaluation of CFD best practices for combustor design: Part I – non-reacting flows, Paper AIAA 2013-1144, 2013.